data

Data Descriptor

Dataset for the Heat-Up and Heat Transfer towards Single Particles and Synthetic Particle Clusters from Particle-Resolved CFD Simulations

Mario Pichler [1,†], Markus Bösenhofer [1,2,*,†] and Michael Harasek [1]

[1] Institute of Chemical, Environmental & Bioscience Engineering, Technische Universität Wien, Getreidemarkt 9/166, 1060 Vienna, Austria; mario.pichler@tuwien.ac.at (M.P.); michael.harasek@tuwien.ac.at (M.H.)
[2] Area 4—Simulation and Analyses, K1-MET GmbH, Stahlstraße 14, 4020 Linz, Austria
* Correspondence: markus.boesenhofer@tuwien.ac.at; Tel.: +43-1-58801-166251
† These authors contributed equally to this work.

Abstract: Heat transfer to particles is a key aspect of thermo-chemical conversion of pulverized fuels. These fuels tend to agglomerate in some areas of turbulent flow and to form particle clusters. Heat transfer and drag of such clusters are significantly different from single-particle approximations commonly used in Euler–Lagrange models. This fact prompted a direct numerical investigation of the heat transfer and drag behavior of synthetic particle clusters consisting of 44 spheres of uniform diameter (60 µm). Particle-resolved computational fluid dynamic simulations were carried out to investigate the heat fluxes, the forces acting upon the particle cluster, and the heat-up times of particle clusters with multiple void fractions (0.477–0.999) and varying relative velocities (0.5–25 m/s). The integral heat fluxes and exact particle positions for each particle in the cluster, integral heat fluxes, and the total acting force, derived from steady-state simulations, are reported for 85 different cases. The heat-up times of individual particles and the particle clusters are provided for six cases (three cluster void fractions and two relative velocities each). Furthermore, the heat-up times of single particles with different commonly used representative particle diameters are presented. Depending on the case, the particle Reynolds number, the cluster void fraction, the Nusselt number, and the cluster drag coefficient are included in the secondary data.

Dataset: 10.17632/97y842jr5m.1.

Dataset License: Creative Commons Attribution 4.0 International (CC BY 4.0).

Keywords: particle resolved simulations; convective heat flux; radiative heat flux; drag forces; particle cluster; particle temperatures

Citation: Pichler, M.; Bösenhofer, M.; Harasek, M. Dataset for the Heat-Up and Heat Transfer towards Single Particles and Synthetic Particle Clusters from Particle-Resolved CFD Simulations. *Data* **2022**, *7*, 23. https://doi.org/10.3390/data7020023

Academic Editor: Yongqing Cai

Received: 11 January 2022
Accepted: 10 February 2022
Published: 14 February 2022

1. Summary

Virtual prototyping and digital twins of industrial processes for investigation and optimization have become increasingly popular with increasing computational power. Pulverized coal boilers [1,2] and blast furnaces [3,4] show great potential for optimization using computational investigations. In both cases, pulverized fuel particles are injected into the furnace, where the thermo-chemical conversion starts immediately. Even though computational power has increased drastically in recent years, the fully resolved simulation of most industrial-scale processes is still not viable. In order to enable simulations of these processes, assumptions and simplifications need to be made.

For pulverized coal and blast furnaces, a common approach for modeling the pulverized fuel particles is the Eulerian–Lagrange (EL) approach. In EL models, the carrier phase is described as an Eulerian phase, while the fuel particles are tracked as Lagrangian particles. Usually, particles are lumped into parcels to reduce the computational effort. The parcels are assumed to consist of an arbitrary number of particles with a single representative size [5,6]. Heat transfer, mass transfer, and particle drag are calculated based on the representative particle diameter for each parcel, neglecting any agglomeration or grouping effects. It is essential to consider flow shielding, radiation shading, and other inter-particle effects to predict the particle heat up and the thermo-chemical conversion within particle clouds or dense particle jets correctly [7–14].

Lu et al. [15] used two immersed boundary methods to simulate the gas–solid heat transfer of dense particle packing in tubes. They provide plots of the heat transfer coefficients for each of the up-to-570 particles in the packing and for Reynolds numbers of up to 1800. They observed that the heat transfer coefficients of particles located at the fluid entrance section of the packing are higher than those located further downstream.

The particle resolved Viscous Penalty Method (VPM) was used by Chadil et al. [16] to determine the local and global Nusselt numbers of single spheres, a regular face-centered cubic array of spheres, and randomly arranged spheres. A good agreement of the global Nusselt number compared with different established correlations was found for low Reynolds numbers (Re = 50 and 100) and void fractions of ϕ = 0.4–0.95.

The influence of the Reynolds number and void fraction on the overall convective heat transfer in randomly distributed arrays of spherical and sphero-cylindrical particles was shown by Tavassoli et al. [17] and Tavassoli et al. [18], respectively. For $Re < 180$, the authors provide plots of the Nusselt numbers for three and six void fractions for spheres and sphero-cylinders, respectively.

All of the mentioned studies show how convective heat transfer is influenced by the relative velocity and the void fraction of clustered particles. Radiative heat transfer is neglected in all of them. None of the mentioned studies provide detailed and comprehensive information about the heat transfer or heat-up times of the individual particles in the arrangement. In most studies, the data are only presented graphically and are thus hard to retrieve and re-use.

Yin [19] shows the importance of particle radiation in pulverized coal-fired utility boilers. They state that an accurate description of the particles' emissivity and scattering properties influences the temperature and reaction extend of the coal particles, the temperature profiles in the furnace, and thus the entire combustion process. Possible particle clustering effects are not taken into account.

To evaluate the effect of particle clustering on the heat transfer, heat-up, and drag behavior of pulverized fuels in high-temperature environments, clusters with various cluster void fractions were constructed. Using particle-resolved direct numerical simulation synthetic particle clusters with various cluster void fractions at different relative velocities, we derived models that do consider particle clustering effects in EL simulations in the main research paper: Bösenhofer et al. [20]. A detailed description of the data gathered in [20] is presented here.

The data set presented in the current work includes additional information about convective and radiative heat fluxes, averaged particle temperatures, and the particle position of each particle in the cluster. The data presented in this article can help understand the convective and radiative heat transfer, and drag behavior of single particles in a clustered arrangement and particle clusters at void fractions close to packed beds up to single spheres. Heat transfer and drag models can be derived from the data. The influence of flow shading and radiation shielding on the heat transfer and particle heat-up depending on the particle's position in the cluster can be investigated. Thus, the presented data have the potential to improve the simulation of heat transfer in any turbulent gas–solid flow where clustering effects occur. These phenomena include, among others, pulverized particle combustion, pulverized carbon carrier injection in iron making, or pharmaceutical and chemical processes. Correct heat transfer prediction and the associated improvements of the modeling results provide a huge potential to reduce the overall emission and to improve efficiencies of the target processes. The full dataset is available in Mendeley Data [21].

2. Data Description

The data presented in this work consist of the primary dataset (averaged simulated raw data) and secondary dataset, which is derived from the primary dataset.

2.1. Primary Dataset

The primary dataset represents three different computational fluid dynamics (CFD) simulations:

1. Steady-state simulations (ST) of the flow around particle clusters (dataset 1, Table 1);
2. Transient simulations (T) of the flow around particle clusters, including particle heat-up (dataset 2);
3. Transient simulation of the flow around single spheres, including particle heat up (dataset 3).

As the raw data of a single case are too big to be presented here, the averaged particle temperatures, and integral heat fluxes and forces are provided here.

ad 1

The primary dataset consists of the data presented in Table 1 and the data provided in dataset 1.

Dataset 1 contains the case id, the exact position of particles in the cluster, the integral convective heat flux $\dot{Q}_{conv}$ (in mW), and the integral radiative heat flux $\dot{Q}_{rad}$ (in mW) for each individual particle in the cluster. The case id, relative velocity U_{rel} (in m/s), the distance between particles (in µm), the integral convective heat flux $\dot{Q}_{conv}$, the integral radiative heat flux $\dot{Q}_{rad}$ for the whole particle cluster, and the net force in flow direction F acting upon the particle cluster (in µN) are presented in Table 1.

As the velocity of the particle clusters is zero, the relative velocity in Table 1 is the superficial velocity. The distance between particles is defined as the distance between particle centers. The convective and radiative heat fluxes are given as absolute values. Here, as the temperature of particles is lower than the temperature of the surroundings, $\dot{Q}_{conv}$ and $\dot{Q}_{rad}$ are the total heat fluxes from the surroundings to the particles or the cluster. The fluxes and forces presented in Table 1 are the integrated heat fluxes over all particles. The integrated heat fluxes for each individual particle and the exact particle position in the cluster are provided in dataset 1 for all cases ST1–ST85. Particle positions are given relative to the reference sphere marked in Figure 1. Cases ST61–ST65 represent single sphere simulations. Cases ST66–ST85 are simulations of random clusters with a particle size distribution (PSD) according to the Weibull distribution [22].

ad 2

Dataset 2 contains the mass averaged temperature profile (in K) and the exact position of each individual particle in the cluster for conditions given in Table 2. The data are provided for simulation with and without radiation-coupled regions.

ad 3

Dataset 3 contains the mass averaged sphere temperature profile (in K) of size equivalent (SE), mass equivalent (ME), area equivalent (AE), and area and mass equivalent (AME) single-sphere simulations. Simulation conditions are shown in Table 3.

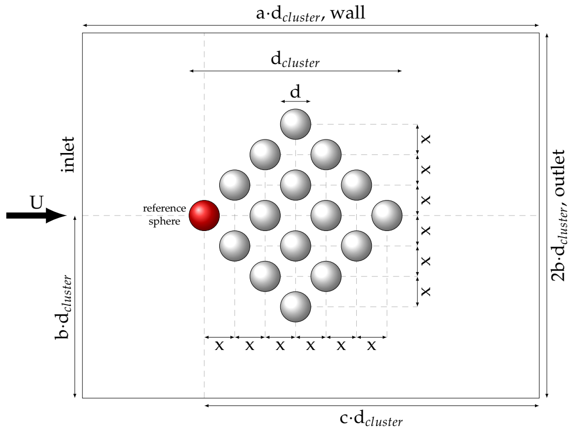

Figure 1. Horizontal cross section of the particle cluster: 2·x is the distance between the particle centers, which is varied to obtain clusters with different void fractions. Cuts through all Cartesian axis planes look identical. The scaling factors of the simulation domain are a = 12, b = 3.75, and c = 10. Adapted from [20].

2.2. Secondary Dataset

The secondary dataset contains additional information, derived from the primary dataset. This includes the particle Reynolds number Re_P (all cases), the cluster void fraction ϕ (cases ST1–ST85 and T1–T6), the Nusselt number Nu, and the cluster drag coefficient ξ (cases ST1–ST85). Secondary data are included in Tables 1–3.

Table 1. Summary particle cluster variations. Cases ST61–ST65 represent single sphere simulations. Cases ST66–ST85 are simulations of random clusters.

Case ID	U_{rel} (m/s)	Distance 2·x (µm)	$\dot{Q}_{conv}$ (mW)	$\dot{Q}_{rad}$ (mW)	F (µN)	ϕ (-)	Re_P (-)	Nu (-)	ξ (-)
ST1	0.5	95	12.44	33.67	0.107	0.477	0.29	0.208	9.937
ST2	1	95	13.35	33.79	0.259	0.477	0.58	0.223	6.014
ST3	5	95	18.26	33.98	1.890	0.477	2.88	0.305	1.753
ST4	13	95	24.02	33.93	7.263	0.477	7.5	0.401	0.996
ST5	25	95	29.88	33.93	19.467	0.477	14.42	0.499	0.722
ST6	0.5	100	12.97	36.28	0.112	0.552	0.29	0.217	10.351
ST7	1	100	13.91	36.48	0.272	0.552	0.58	0.232	6.312
ST8	5	100	19.14	36.74	1.989	0.552	2.88	0.32	1.845
ST9	13	100	25.23	36.74	7.685	0.552	7.5	0.422	1.054
ST10	25	100	31.50	36.75	20.721	0.552	14.42	0.526	0.769
ST11	0.5	110	13.91	41.07	0.120	0.663	0.29	0.232	11.104
ST12	1	110	15.04	40.81	0.295	0.663	0.58	0.251	6.832
ST13	5	110	20.88	41.04	2.186	0.663	2.88	0.349	2.027
ST14	13	110	27.71	40.99	8.558	0.663	7.5	0.463	1.174
ST15	25	110	34.95	41.00	23.360	0.663	14.42	0.584	0.867
ST16	0.5	120	15.05	44.15	0.131	0.741	0.29	0.251	12.117
ST17	1	120	16.21	44.04	0.319	0.741	0.58	0.271	7.394
ST18	5	120	22.64	44.34	2.408	0.741	2.88	0.378	2.233
ST19	13	120	30.32	44.32	9.539	0.741	7.5	0.507	1.309
ST20	25	120	38.86	44.32	26.380	0.741	14.42	0.649	0.979

Table 1. *Cont.*

Case ID	U_{rel} (m/s)	Distance 2·x (μm)	$\dot{Q}_{conv}$ (mW)	$\dot{Q}_{rad}$ (mW)	F (μN)	ϕ (-)	Re_P (-)	Nu (-)	ξ (-)
ST21	0.5	130	15.91	46.80	0.136	0.796	0.29	0.266	12.622
ST22	1	130	17.32	46.63	0.335	0.796	0.58	0.289	7.765
ST23	5	130	24.50	46.82	2.595	0.796	2.88	0.409	2.407
ST24	13	130	33.11	46.78	10.417	0.796	7.5	0.553	1.429
ST25	25	130	43.36	46.79	29.175	0.796	14.42	0.725	1.082
ST26	0.5	150	17.98	51.60	0.152	0.867	0.29	0.3	14.11
ST27	1	150	19.68	51.87	0.371	0.867	0.58	0.329	8.599
ST28	5	150	28.30	52.00	3.018	0.867	2.88	0.473	2.799
ST29	13	150	39.53	51.96	12.437	0.867	7.5	0.661	1.706
ST30	25	150	54.44	51.97	35.616	0.867	14.42	0.91	1.321
ST31	0.5	170	20.02	56.19	0.168	0.909	0.29	0.335	15.543
ST32	1	170	22.01	56.80	0.408	0.909	0.58	0.368	9.455
ST33	5	170	32.26	56.91	3.454	0.909	2.88	0.539	3.203
ST34	13	170	46.41	56.88	14.577	0.909	7.5	0.776	2
ST35	25	170	68.67	56.89	42.449	0.909	14.42	1.147	1.575
ST36	0.5	190	22.09	60.58	0.184	0.935	0.29	0.369	17.046
ST37	1	190	24.36	61.27	0.450	0.935	0.58	0.407	10.425
ST38	5	190	36.13	61.84	3.907	0.935	2.88	0.604	3.624
ST39	13	190	54.56	61.82	16.840	0.935	7.5	0.912	2.311
ST40	25	190	85.11	61.82	49.511	0.935	14.42	1.422	1.837
ST41	0.5	243	27.13	69.11	0.226	0.969	0.29	0.453	20.925
ST42	1	243	30.39	69.54	0.571	0.969	0.58	0.508	13.242
ST43	5	243	48.25	69.78	5.138	0.969	2.88	0.806	4.765
ST44	13	243	81.44	69.71	22.742	0.969	7.5	1.361	3.12
ST45	25	243	126.84	69.75	65.175	0.969	14.42	2.12	2.418
ST46	0.5	415	42.53	75.34	0.381	0.994	0.29	0.711	35.376
ST47	1	415	47.25	72.91	0.924	0.994	0.58	0.817	21.421
ST48	5	415	86.07	72.90	8.582	0.994	2.88	1.51	7.96
ST49	13	415	123.93	72.98	33.143	0.994	7.5	2.269	4.547
ST50	25	415	151.88	73.02	65.175	0.994	14.42	2.852	2.999
ST51	0.5	523	50.73	76.45	0.464	0.997	0.29	0.848	43.021
ST52	1	523	59.50	76.55	1.112	0.997	0.58	0.994	25.784
ST53	5	523	107.17	76.80	9.788	0.997	2.88	1.791	9.079
ST54	13	523	146.13	76.75	34.939	0.997	7.5	2.442	4.794
ST55	25	523	176.33	76.77	82.860	0.997	14.42	2.947	3.074
ST56	0.5	892	73.07	77.40	0.650	0.999	0.29	1.221	60.304
ST57	1	892	86.13	77.46	1.541	0.999	0.58	1.439	35.732
ST58	5	892	126.38	77.60	11.153	0.999	2.88	2.112	10.345
ST59	13	892	155.00	77.56	36.614	0.999	7.5	2.59	5.024
ST60	25	892	181.95	77.63	85.594	0.999	14.42	3.041	3.176
ST61	0.5	-	2.56	1.67	0.023	1.0	0.29	1.881	93.069
ST62	1	-	2.67	1.71	0.046	1.0	0.58	1.96	46.797
ST63	5	-	3.11	1.77	0.272	1.0	2.88	2.289	11.107
ST64	13	-	3.70	1.77	0.877	1.0	7.5	2.718	5.293
ST65	25	-	4.34	1.77	2.056	1.0	14.42	3.189	3.357
ST66	0.5	random	69.191	424.35	0.479	0.935	0.55	0.337	6.79
ST67	1	random	81.276	426.044	1.533	0.935	1.1	0.396	5.432
ST68	5	random	148.308	426.835	16.824	0.935	5.5	0.723	2.385
ST69	13	random	272.243	426.59	79.151	0.935	14.31	1.327	1.660
ST70	25	random	414.315	426.671	231.505	0.935	27.51	2.020	1.313

Table 1. *Cont.*

Case ID	U_{rel} (m/s)	Distance 2·x (µm)	$\dot{Q}_{conv}$ (mW)	$\dot{Q}_{rad}$ (mW)	F (µN)	ϕ (-)	Re_P (-)	Nu (-)	ξ (-)
ST71	0.5	random	49.13	246.538	0.342	0.935	0.55	0.419	8.508
ST72	1	random	56.543	246.799	1.078	0.935	1.1	0.482	6.694
ST73	5	random	97.819	248.35	10.987	0.935	5.5	0.835	2.730
ST74	13	random	173.922	248.247	50.813	0.935	14.31	1.484	1.868
ST75	25	random	263.083	248.362	147.545	0.935	27.51	2.245	1.466
ST76	0.5	random	53.215	269.667	0.388	0.935	0.55	0423	8.981
ST77	1	random	61.628	270.173	1.142	0.935	1.1	0.490	6.602
ST78	5	random	112.043	271.776	12.243	0.935	5.5	0.891	2.831
ST79	13	random	198.243	271.734	55.261	0.935	14.31	1.576	1.890
ST80	25	random	285.621	271.82	153.915	0.935	27.51	2.270	1.423
ST81	0.5	random	53.154	291.935	0.360	0.935	0.55	0.372	7.328
ST82	1	random	61.436	292.783	1.109	0.935	1.1	0.430	5.648
ST83	5	random	105.758	294.213	11.465	0.935	5.5	0.741	2.336
ST84	13	random	182.935	294.125	52.640	0.935	14.31	1.282	1.587
ST85	25	random	283.918	294.176	154.529	0.935	27.51	1.989	1.260

Table 2. Summary of transient cluster heat-up cases (dataset 2). Adapted from [20].

Case ID	U_{rel} (m/s)	Re_P (-)	ϕ (-)	Distance 2·x (µm)
T1	0.5	0.29	0.552	100
T2	13	7.50	0.552	100
T3	0.5	0.29	0.741	120
T4	13	7.50	0.741	120
T5	0.5	0.29	0.935	190
T6	13	7.50	0.935	190

Table 3. Summary of transient single sphere heat-up cases (dataset 3). Adapted from [20].

Case ID	U_{rel} (m/s)	d_P (µm)	Re_P (-)	m (kg)
SE1	0.5	60	0.29	1.24×10^{-10}
SE2	13	60	7.50	1.24×10^{-10}
ME1	0.5	211.8	1.02	5.47×10^{-9}
ME2	13	211.8	26.46	5.47×10^{-9}
AE1	0.5	397.8	1.91	3.63×10^{-8}
AE2	13	397.8	49.70	3.63×10^{-8}
AME1	0.5	397.8	1.91	5.47×10^{-9}
AME2	13	397.8	49.70	5.47×10^{-9}

3. Methods

3.1. Simulation Setup and Conditions

The synthetic particle clusters were constructed as regular rhomboid-shaped to enable a systematic approach. The distance between particles was varied to evaluate the influence of the cluster void fraction on the drag and heat transfer behavior. Void fractions were chosen to close the gap from loosely packed beds (void fraction ϕ = 0.477) to single particles in cross flow ($\phi \rightarrow 1$). This range of void fractions represents solid-to-gas mass ratios of 1737 to 1 for ϕ = 0.477 to 0.999, respectively. For pulverized fuel particles injected by dense-phase pneumatic conveying, the initial solid-to-gas mass ratio can exceed 100 [23–26]. It is known that particles tend to cluster randomly in turbulent flows [8,27,28]. To account for this, simulations for four randomly shaped particle clusters with a fixed void fraction consisting of spheres with a particle size distribution according to the Weibull distribution were carried out.

The data were gathered from particle resolved direct numerical simulations using the open-source CFD toolbox OpenFOAM® v7 [29]. The particles were fixed in space to avoid numerical expensive moving and deforming meshes in the simulations and to allow for the investigation of different relative velocities. The numerical meshes consist of a base cell size of 60 μm, with significant refinement in the wake of the cluster and towards the particles, resulting in up to 14 million cells. Simulations were carried out using the *chtMultiRegionFoam* solver, which couples fluid and solid regions explicitly in space and time. Radiation was modeled by the finite volume discrete ordinates model (fvDOM) [30] with 16 discrete rays. Gas phase radiation was modeled by gray mean absorption [31]. The boundary conditions are summarized in Table 4. A uniform fixed value was set for the velocity at the inlet patch, while a zero gradient, no slip and slip boundary condition was set at the outlet, the particles, and the remaining patches, respectively. The pressure was set to a fixed value at the outlet. A zero gradient boundary condition was used for all other patches. The temperature was fixed at the fluid inlet, while a zero gradient condition was imposed at all other patches. The particle surface temperature was set to a uniform fixed value in all steady-state simulations (ST1–ST85). For particle and cluster heat-up simulations (SE, ME, AE, AME single-sphere simulations, and T1–T6), a coupled boundary condition was used. This boundary condition couples the diffusive, convective, and radiative heat fluxes between the solid and fluid regions. All surfaces were treated as gray bodies with an emissivity of $\epsilon = 1$. The inlet velocity was varied based on values given in Tables 1–3. The temperature of the gas at the inlet was set to 2500 K, and the pressure at the outlet was fixed to 5 $\text{bar}_{(a)}$. In ST1–ST85, the particle temperature was fixed to a value 2450 K. The initial temperature of particles in the transient simulations was set to 400 K.

The thermo-physical properties of the GRI3.0 mechanism [32] were applied for the gas phase species, while particle properties were kept constant (Table 5).

Single-sphere simulations for dataset 3 used the same case setup as the cluster simulations, with the exception of the cluster being replaced by a single sphere with diameter according to Table 3. The different sphere diameters present different commonly used representative particle diameters. Here, the particle clusters were substituted by a single particle with one of the following:

1. A size equivalent sphere (SE): The single-sphere diameter is equal to the size of the particles in the cluster (d = 60 μm);
2. A mass equivalent sphere (ME): The single-sphere mass is equal to the mass of the cluster (d = 211.8 μm);
3. A surface area equivalent sphere (AE): The single-sphere surface area is equal to the surface area of the cluster (d = 397.8 μm);
4. A surface and mass equivalent sphere (AME): The single-sphere surface area and mass are equal to the cluster. The sphere diameter is equal to the AE case, but the particle density is reduced to 165.8 kg/m^3.

A cross section of the cluster's simulation domain is shown in Figure 1. The size of the simulation domain in the cluster simulation was scaled with the cluster diameter $d_{cluster}$ using the constant scaling factors a, b, and c. The inlet velocity and cluster void fraction were varied according to Tables 1 and 2. A constant particle diameter of 60 μm was used in the cluster simulations, except for cases ST66–ST85, where a PSD was used.

Table 4. Summary boundary conditions. Adapted from [20].

Patch	U	p	T	I
inlet	fixed value	zero gradient	fixed value	gray body
outlet	zero gradient	fixed value	zero gradient	gray body
wall	slip	zero gradient	zero gradient	gray body
fluid to solid	no slip	zero gradient	coupled	gray body

Table 5. Gas phase composition and thermo-physical properties as well as solid thermo-physical properties used in the simulations. Adapted from [20].

Bulk Gas Phase Thermo-Physical Properties	
density (ρ)	0.69 kg/m^3
specific heat capacity (c_p)	1300 J/(kg K)
thermal conductivity (κ)	0.133 W/(m K)
viscosity (μ)	7.213$\cdot$10^{-5} Pa s
Solid Thermo-Physical Properties	
density (ρ)	1100 kg/m^3
emissivity (ε)	1
specific heat capacity (c_p)	1660 J/(kg K)
thermal conductivity (κ)	1.241 W/(m K)

The resulting velocity and temperature field and the velocity and temperature contours in the horizontal cross section for cases ST4, ST29, ST59, and ST69 are shown in Figures 2–5. Note that the whole cluster and not only the horizontal cross section is shown. Due to the file size for each case, the computational meshes and the respective fields cannot be provided.

The convective ($\dot{Q}_{conv}$) and radiative ($\dot{Q}_{rad}$) heat fluxes of each sphere in the particle cluster for cases ST1–ST5, ST26–ST30, ST56–ST60, and ST66–ST70 are shown in Figure 6a–d, respectively.

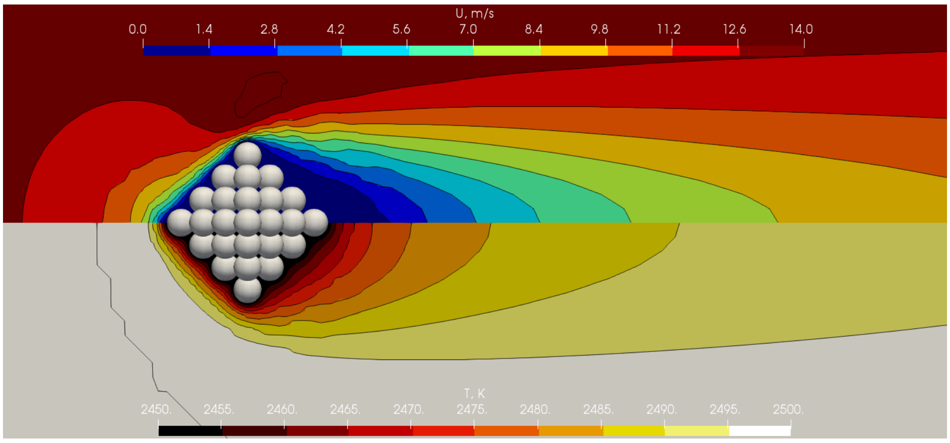

Figure 2. Graphical representation of the full cluster, velocity field, temperature field, and the respective contours in the horizontal cross section for case ST4.

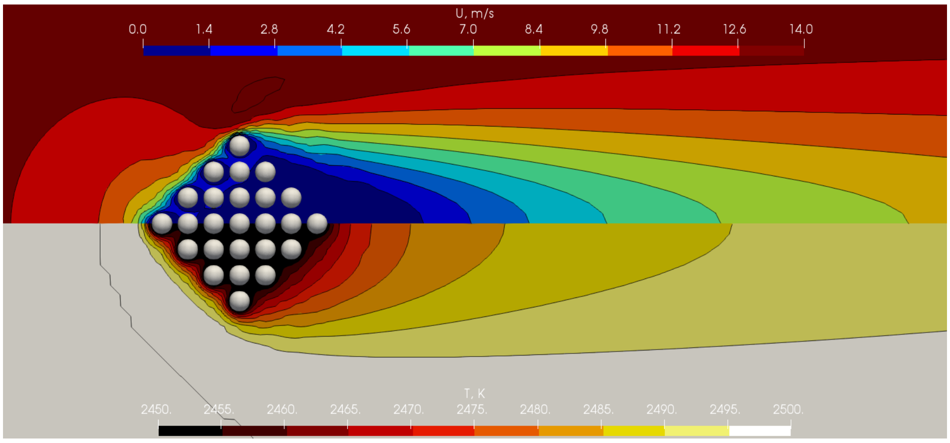

Figure 3. Graphical representation of the full cluster, velocity field, temperature field, and the respective contours in the horizontal cross section for case ST29.

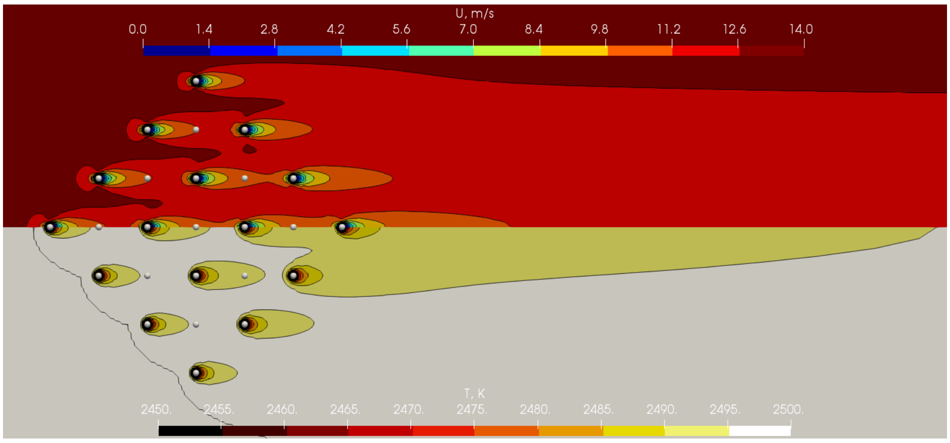

Figure 4. Graphical representation of the full cluster, velocity field, temperature field, and the respective contours in the horizontal cross section for case ST59.

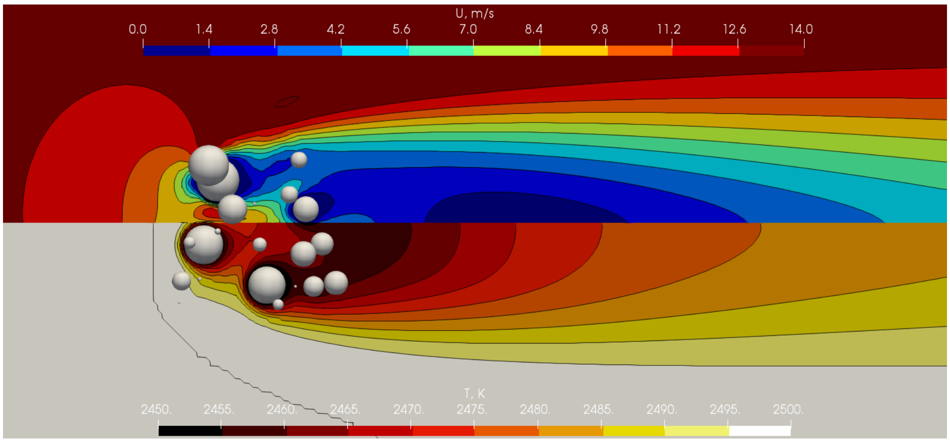

Figure 5. Graphical representation of the full cluster, velocity field, temperature field, and the respective contours in the horizontal cross section for case ST69.

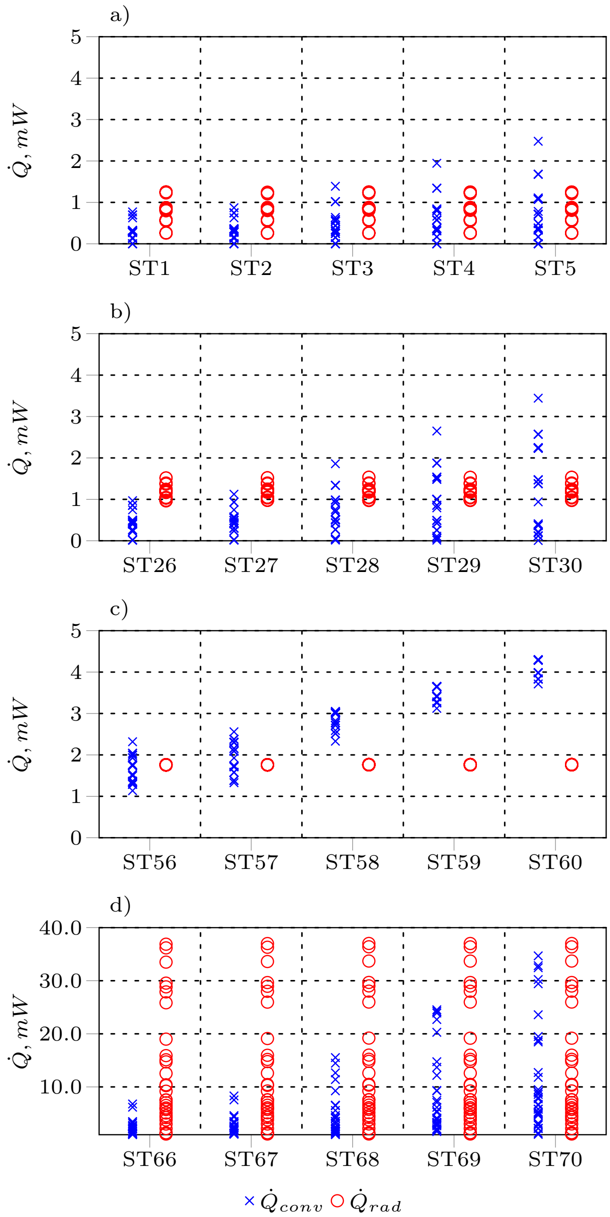

Figure 6. Convective and radiative heat fluxes of each sphere in a cluster for different cases. (**a**) ST1–ST5, ϕ = 0.477, U_{rel} = 0.5–25 m/s; (**b**) ST26–ST30, ϕ = 0.867, U_{rel} = 0.5–25 m/s; (**c**) ST56–ST60, ϕ = 0.999, U_{rel} = 0.5–25 m/s; and (**d**) ST66–ST70, ϕ = 0.935, U_{rel} = 0.5–25 m/s.

3.2. Data Collection

Simulations ST1–ST85 were evaluated after a steady state was reached (steady value of the drag force and heat transfer rates). Transient simulations were carried out until the mean particle temperatures were close to the gas temperature (2500 K).

The cluster void fraction was calculated from Equation (1), where d is the particle diameter, x is half the distance between sphere centers (Figure 1), and 17.8251 is the graphically determined number of full spheres in the considered volume (the biggest possible rhomboid through the particle centers).

The particle temperature was calculated from the simulated cell values as the mass-weighted average using Equation (2), where ρ is the particle density, V is the cell volume, T is the cell temperature, and N is the number of cells in the particle.

$$\phi = 1 - \frac{V_{solid}}{V_{tot}} = 1 - \frac{17.8251\frac{d^3\pi}{6}}{36x^3} \quad (1)$$

$$T_{av} = \frac{\sum_{i=1}^{N}(\rho_i V_i T_i)}{\sum_i(\rho_i V_i)} \quad (2)$$

The particle Reynolds number Re_P, Nusselt number Nu, and the drag coefficient ξ are calculated from Equations (3)–(5), respectively [33,34]. Here, $\dot{Q}_{conv}$ is the integrated cluster heat flux, T_∞ is the gas temperature at the inlet, T is the mass averaged cluster (dataset 1 and dataset 2) or particle (dataset 3) temperature, κ is the thermal conductivity of the gas, $A_{CL,S}$ is the cluster (dataset 1 and dataset 2) or particle (dataset 3) surface area, and A_{CL} is the cluster cross-sectional area. All thermo-physical gas properties are calculated at 2500 K and 5 bar$_{(a)}$. Cases ST61–ST65 are the simulations of a single sphere in cross-flow. Cases ST66–ST85 represent random clusters with a particle size distribution according to the Weibull distribution (Equation (6)) [22] with a shape parameter of k = 1.14 and a scale parameter of λ = 120 µm. The diameter used to calculate Re_P in Table 1 is the first moment of the PSD: $\bar{d} = \int_{d_{min}}^{d_{max}} d\, q(d)\, \mathrm{d}d$ = 114.5 µm.

$$Re_P = \frac{\rho U d}{\mu} \quad (3)$$

$$Nu = \frac{\dot{Q}_{conv}\, d}{A_S\, \kappa(T_\infty - T)} \quad (4)$$

$$\xi = \frac{F}{\rho \frac{U^2}{2} A_{CL}} \quad (5)$$

$$q(d) = \frac{k}{\lambda}\left(\frac{d}{\lambda}\right)^{k-1} \cdot exp\left(-\left(\frac{d}{\lambda}\right)^{k}\right) \quad (6)$$

Author Contributions: Conceptualization, M.B.; methodology, M.B. and M.P.; software, M.B. and M.P.; validation, M.B. and M.P.; formal analysis, M.B.; investigation, M.B. and M.P.; resources, M.B. and M.P.; data curation, M.B. and M.P.; writing—original draft preparation, M.P.; writing—review and editing, M.B., M.P., and M.H.; visualization, M.B. and M.P.; supervision, M.H.; project administration, M.H.; funding acquisition, M.H. All authors have read and agreed to the published version of the manuscript.

Funding: This research was funded by FFG (Austrian Research Promotion Agency), grant numbers 844607 and 86929. The APC was funded by TU Wien Bibliothek. (Open Access Funding by TU Wien).

Institutional Review Board Statement: Not applicable.

Informed Consent Statement: Not applicable.

Data Availability Statement: The data presented in this study are openly available in Mendeley Data (10.17632/97y842jr5m.1, accessed on 10 January 2022) under the CC BY 4.0 licence.

Acknowledgments: The authors gratefully acknowledge the funding support of the K1-MET GmbH, metallurgical competence center. The research program of the competence center K1-MET is supported by COMET (Competence Center for Excellent Technologies), the Austrian program for competence centers. COMET is funded by the Federal Ministry for Transport, Innovation, and Technology; the Federal Ministry for Science, Research, and Economy; the provinces of Upper Austria, Tyrol, and Styria; and the Styrian Business Promotion Agency. The computational results presented have been achieved in part using the Vienna Scientific Cluster (VSC). The authors acknowledge the TU Wien University Library for financial support through its Open Access Funding Programme.

Conflicts of Interest: The authors declare no conflict of interest.

Abbreviations

The following abbreviations are used in this manuscript:

AE	Surface area equivalent
AME	Surface area and mass equivalent
CFD	Computational fluid dynamics
fvDOM	Finite volume discrete ordinates model
ME	Mass equivalent
PSD	Particle size distribution
SE	Size equivalent
ST	Steady-state simulation
T	Transient simulation

References

1. Prokhorov, D.A.; Piralishvili, S.A. Numerical simulation of pulverized coal combustion and comparison with in-furnace measurements. *AIP Conf. Proc.* **2020**, *2211*, 040008. [CrossRef]
2. Zheng, J.; Liu, P.; Shen, Z. Simulation of Turbulent Combustion in a Large Pulverized Coal Boiler Based on Turbulent Radiation Interaction and the Modified Soot Model. *ACS Omega* **2020**, *5*, 23822–23835. [CrossRef] [PubMed]
3. Kuang, S.; Li, Z.; Yu, A. Review on Modeling and Simulation of Blast Furnace. *Steel Res. Int.* **2018**, *89*, 1700071. [CrossRef]
4. Abhale, P.B.; Viswanathan, N.N.; Saxén, H. Numerical modelling of blast furnace—Evolution and recent trends. *Miner. Process. Extr. Metall.* **2020**, *129*, 166–183. [CrossRef]
5. Zhong, W.; Yu, A.; Zhou, G.; Xie, J.; Zhang, H. CFD simulation of dense particulate reaction system: Approaches, recent advances and applications. *Chem. Eng. Sci.* **2016**, *140*, 16–43. [CrossRef]
6. Zhou, L. *Theory and Modeling of Dispersed Multiphase Turbulent Reacting Flows*; Butterworth-Heinemann: Oxford, UK, 2018.
7. Haugen, N.E.L.; Mitchell, R.E. Modeling radiation in particle clouds: On the importance of inter-particle radiation for pulverized solid fuel combustion. *Heat Mass Transf.* **2015**, *51*, 991–999. [CrossRef]
8. Banko, A.J.; Villafañe, L.; Kim, J.H.; Esmaily, M.; Eaton, J.K. Stochastic modeling of direct radiation transmission in particle-laden turbulent flow. *J. Quant. Spectrosc. Radiat. Transf.* **2019**, *226*, 1–18. [CrossRef]
9. Forgber, T.; Radl, S. A novel approach to calculate radiative thermal exchange in coupled particle simulations. *Powder Technol.* **2018**, *323*, 24–44. [CrossRef]
10. Liberman, M.A.; Kleeorin, N.; Rogachevskii, I.; Haugen, N.E.L. Multipoint radiation induced ignition of dust explosions: Turbulent clustering of particles and increased transparency. *Combust. Theory Model.* **2018**, *22*, 1084–1102. [CrossRef]
11. Bermúdez, A.; Ferrín, J.; Liñán, A.; Saavedra, L. Numerical simulation of group combustion of pulverized coal. *Combust. Flame* **2011**, *158*, 1852–1865. [CrossRef]
12. Haugen, N.E.L.; Krüger, J.; Mitra, D.; Løvås, T. The effect of turbulence on mass transfer rates of small inertial particles with surface reactions. *J. Fluid Mech.* **2018**, *836*, 932–951. [CrossRef]
13. Krüger, J.; Haugen, N.E.L.; Løvås, T. Correlation effects between turbulence and the conversion rate of pulverized char particles. *Combust. Flame* **2017**, *185*, 160–172. [CrossRef]
14. Krüger, J.; Haugen, N.E.; Mitra, D.; Løvås, T. The effect of turbulent clustering on particle reactivity. *Proc. Combust. Inst.* **2017**, *36*, 2333–2340. [CrossRef]
15. Lu, J.; Zhu, X.; Peters, E.; Verzicco, R.; Lohse, D.; Kuipers, J. Moving from momentum transfer to heat transfer—A comparative study of an advanced Graetz-Nusselt problem using immersed boundary methods. *Chem. Eng. Sci.* **2019**, *198*, 317–333. [CrossRef]
16. Chadil, M.A.; Vincent, S.; Estivalèzes, J.L. Gas-Solid Heat Transfer Computation from Particle-Resolved Direct Numerical Simulations. *Fluids* **2022**, *7*, 15. [CrossRef]
17. Tavassoli, H.; Kriebitzsch, S.; van der Hoef, M.; Peters, E.; Kuipers, J. Direct numerical simulation of particulate flow with heat transfer. *Int. J. Multiph. Flow* **2013**, *57*, 29–37. [CrossRef]
18. Tavassoli, H.; Peters, E.; Kuipers, J. Direct numerical simulation of fluid-particle heat transfer in fixed random arrays of non-spherical particles. *Chem. Eng. Sci.* **2015**, *129*, 42–48. [CrossRef]
19. Yin, C. On gas and particle radiation in pulverized fuel combustion furnaces. *Appl. Energy* **2015**, *157*, 554–561. [CrossRef]
20. Bösenhofer, M.; Pichler, M.; Harasek, M. Heat Transfer Models for Dense Pulverized Particle Jets. *Processes* **2022**, *10*, 238. [CrossRef]
21. Pichler, M.; Bösenhofer, M.; Harasek, M. Dataset for the heat-up and heat transfer towards single particles and synthetic particle clusters from particle resolved CFD simulations. *Mendeley Data* **2022**. [CrossRef]
22. Papoulis, A.; Pillai, S.U. *Probability, Random Variables, and Stochastic Processes*, 4th ed.; McGraw-Hill Series in Electrical and Computer Engineering; McGraw-Hill: Boston, MA, USA, 2002.
23. Konrad, K. Dense-phase pneumatic conveying: A review. *Powder Technol.* **1986**, *49*, 1–35. [CrossRef]
24. Cai, L.; Liu, S.; Pan, X.; Guiling, X.; Xiaoping, C.; Changsui, Z. Influence of carbonaceous powders on flow characteristics of dense-phase pneumatic conveying at high pressure. *Exp. Therm. Fluid Sci.* **2014**, *58*, 121–130. [CrossRef]

25. Liang, C.; Xu, P.; Xu, G.; Chen, X.; Zhao, C.; Duan, L. Comparison on Flow Characteristics of Dense-phase Pneumatic Conveying of Biomass Powder and Pulverized coal at High Pressure. *Energy Sources Part A Recover. Util. Environ. Eff.* **2015**, *37*, 583–589. [CrossRef]
26. Jin, Y.; Lu, H.; Guo, X.; Gong, X. Application of CPFD method in the simulation of vertical dense phase pneumatic conveying of pulverized coal. *Powder Technol.* **2019**, *357*, 343–351.
27. Squires, K.D.; Eaton, J.K. Preferential concentration of particles by turbulence. *Phys. Fluids A Fluid Dyn.* **1991**, *3*, 1169–1178. [CrossRef]
28. Balachandar, S.; Eaton, J.K. Turbulent Dispersed Multiphase Flow. *Annu. Rev. Fluid Mech.* **2010**, *42*, 111–133. [CrossRef]
29. Weller, H.G.; Tabor, G.; Jasak, H.; Fureby, C. A tensorial approach to computational continuum mechanics using object-oriented techniques. *Comput. Phys.* **1998**, *12*, 620–631. [CrossRef]
30. Modest, M.F. *Radiative Heat Transfer*, 3rd ed.; Academic Press: New York, NY, USA, 2013.
31. Grosshandler, W.L. *RADCAL: A Narrow-Band Model for Radiation—Calculations in a Combustion Environment*; Technical Note 1402; National Institute of Standards and Technology (NIST): Gaithersburg, MD, USA, 1993.
32. Smith, G.P.; Golden, D.M.; Frenklach, M.; Moriarty, N.W.; Eiteneer, B.; Goldenberg, M.; Bowman, C.T.; Hanson, R.K.; Song, S.; Gardiner, W.C., Jr.; et al. *GRI-Mech*, Version 3.0; Software for Modelling Natural Gas Combustion; University of California: Berkeley, CA, USA, 2018. Available online: http://combustion.berkeley.edu/gri-mech/version30/text30.html (accessed on 10 January 2022).
33. Karwa, R. *Heat and Mass Transfer*, 2nd ed.; Springer: Singapore, 2020. [CrossRef]
34. Baehr, H.D.; Stephan, K. *Wärme- und Stoffübertragung*, 8th ed.; Springer: Berlin/Heidelberg, Germany, 2013. [CrossRef]